

Nanocrystals

Phase Engineering of Cesium Manganese Bromides Nanocrystals with Color-Tunable Emission

Qingkun Kong, Bin Yang,* Junsheng Chen, Ruiling Zhang, Siping Liu, Daoyuan Zheng, Hongling Zhang, Qingtong Liu, Yiyang Wang, and Keli Han*

Abstract: For display applications, it is highly desirable to obtain tunable red/green/blue emission. However, lead-free perovskite nanocrystals (NCs) generally exhibit broadband emission with poor color purity. Herein, we developed a unique phase transition strategy to engineer the emission color of lead-free cesium manganese bromides NCs and we can achieve a tunable red/green/blue emission with high color purity in these NCs. Such phase transition can be triggered by isopropanol: from one dimensional (1D) CsMnBr_3 NCs (red-color emission) to zero dimensional (0D) Cs_3MnBr_5 NCs (green-color emission). Furthermore, in a humid environment both 1D CsMnBr_3 NCs and 0D Cs_3MnBr_5 NCs can be transformed into 0D $\text{Cs}_2\text{MnBr}_4 \cdot 2\text{H}_2\text{O}$ NCs (blue-color emission). $\text{Cs}_2\text{MnBr}_4 \cdot 2\text{H}_2\text{O}$ NCs could inversely transform into the mixture of CsMnBr_3 and Cs_3MnBr_5 phase during the thermal annealing dehydration step. Our work highlights the tunable optical properties in single component NCs via phase engineering and provides a new avenue for future endeavors in light-emitting devices.

Cesium lead halide perovskite CsPbX_3 (X: Cl, Br, I) nanocrystals (NCs) with narrow photoluminescence (PL) emission band have been shown to be good emitters of red, green and blue light.^[1–11] Major issues about these lead halide perovskites are their toxicity and poor stability.^[12] This has triggered the development of lead-free metal halide perovskite NCs. Different lead-free metal halide perovskites NCs with structure similar to lead halide perovskites have been reported, such as ABX_3 , $\text{A}_3\text{B}_2\text{X}_9$, $\text{A}_2\text{B}(\text{I})\text{B}(\text{III})\text{X}_6$ double perovskite and A_2BX_6 , where A is a cation (Cs^+ , Rb^+ or CH_3NH_3^+), B is a lead-free metallic cation (Ag^+ , Sn^{2+} , Bi^{3+} , Sb^{3+} , Sn^{4+} , Zr^{4+} , etc.).^[13–18] However, most of these lead-free

metal halide NCs exhibit broadband PL with poor color purity due to the strong carrier-phonon coupling.^[19,20] For display applications, it is attractive to obtain NCs with color-tunable emission and high color purity. Various preparation methods (e.g. doping, surface passivation, or A site substituted with organic molecule) show great potential to manipulate emission color of lead-free halide perovskites NCs.^[13–17] However, their tunability for the color range and the color purity is limited.^[21–23] So far, to the best of our knowledge, tunable red/green/blue color emission with high color purity has not been achieved for lead-free metal halide NCs.

Herein, for the first time, we report a tunable pure-color red/green/blue emission in lead-free metal halide NCs by modulating the crystal field strengths and coordination sites of cesium manganese bromides NCs through phase engineering. We develop a unique strategy for the selective synthesis of 1D CsMnBr_3 NCs and 0D Cs_3MnBr_5 NCs with pure phase. 1D CsMnBr_3 NCs with an octahedral coordination give a red emission. While 0D Cs_3MnBr_5 NCs with a tetrahedral coordination exhibit a green emission with a high PLQY of 48% and full-width at half-maximum (FWHM) of 43 nm. Furthermore, we found that water could trigger phase transformation process of 1D CsMnBr_3 NCs and 0D Cs_3MnBr_5 NCs to form stable 0D $\text{Cs}_2\text{MnBr}_4 \cdot 2\text{H}_2\text{O}$ NCs with blue emission.

Cesium manganese halide NCs were prepared by using a hot-injection method (details in SI). The crystal structure can be controlled by the molar ratio between $\text{Cs}(\text{OAc})$ and $\text{Mn}(\text{OAc})_2$ during the hot-injection (Figure 1a). Typically, when $\text{Cs}(\text{OAc})$ -to- $\text{Mn}(\text{OAc})_2$ ratio is 1:1.35, 1D CsMnBr_3 NCs are formed. XRD patterns of the as-prepared NCs are consistent with that of standard CsMnBr_3 (PDF card No. 70-1449). Furthermore, the phase structure of CsMnBr_3 NCs is also confirmed by the Rietveld method (Figure 1b). Refinements suggest that CsMnBr_3 NCs have a perovskite structure with the space group of $\text{P}63/\text{mmc}$ and cell parameters ($a = 7.641 \text{ \AA}$, $b = 7.641 \text{ \AA}$, $c = 6.494 \text{ \AA}$, $\alpha = 90^\circ$, $\beta = 90^\circ$, $\gamma = 120^\circ$, as listed in Table S1). Each Mn atom is coordinated by six Br atoms, in which three Br atoms share the plane that bridges the other adjacent Mn atoms. Plane sharing MnBr_6^{4-} units form 1D MnBr_3 chains and Cs^+ ions are located between the chains. Transmission electron microscopy (TEM) image demonstrates that CsMnBr_3 NCs have an average edge length of $18.9 \pm 3.2 \text{ nm}$ (Figures 1c,d). The high-resolution (HR) TEM image of CsMnBr_3 NCs reveals high crystallinity with clear lattice spacing values of 0.208 nm, which is in good agreement with the (031) plane of CsMnBr_3 crystal (Figure 1e). The chemical compositions of the NCs were checked by energy dispersive X-ray spectroscopy (EDS) and the inductively coupled plasma optical emission spectrometry

[*] Q. Kong, R. Zhang, S. Liu, D. Zheng, H. Zhang, Q. Liu, Y. Wang, Prof. Dr. K. Han
 Institute of Molecular Sciences and Engineering, Institute of Frontier and Interdisciplinary Science, Shandong University
 Qingdao 266237 (P. R. China)
 E-mail: klhan@dicp.ac.cn

B. Yang, J. Chen, Prof. Dr. K. Han
 State Key Laboratory of Molecular Reaction Dynamics, Dalian Institute of Chemical Physics, Chinese Academy of Sciences
 Dalian 116023 (P. R. China)
 E-mail: yangbin@dicp.ac.cn

B. Yang, Prof. Dr. K. Han
 University of the Chinese Academy of Sciences
 Beijing 100039 (P. R. China)

 Supporting information and the ORCID identification number(s) for the author(s) of this article can be found under:
<https://doi.org/10.1002/anie.202105413>

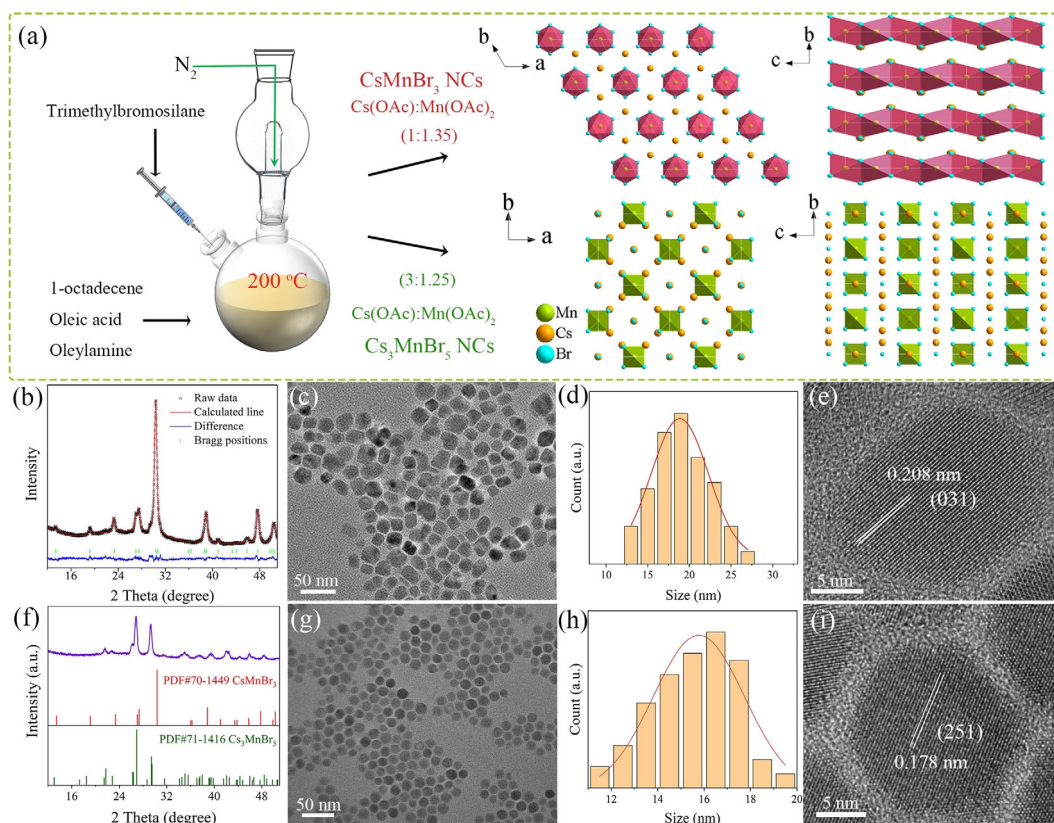


Figure 1. (a) Illustration of the formation process of CsMnBr_3 NCs and Cs_3MnBr_5 NCs. Rietveld refinement XRD patterns of (b) CsMnBr_3 NCs and XRD pattern of (f) as-prepared Cs_3MnBr_5 NCs. The observed data, calculation data, Bragg position and their difference are depicted in Figure 1 b with black cross, red solid line, green line and blue solid line, respectively. TEM images of the obtained (c) CsMnBr_3 NCs and (g) as-prepared Cs_3MnBr_5 NCs. Size distribution histograms of (d) CsMnBr_3 NCs and (h) as-prepared Cs_3MnBr_5 NCs. HRTEM images of a single (e) CsMnBr_3 NCs and (i) as-prepared Cs_3MnBr_5 NCs.

(ICP-OES). The results reveal that the elements are evenly distributed in CsMnBr_3 NCs (Figure S1) and the actual Cs/Mn molar ratio is 0.9:1 (Table S2), which is consistent with the stoichiometry (1:1). These results suggest the successful synthesis of CsMnBr_3 perovskite NCs.

On the other hand, 0D Cs_3MnBr_5 NCs can be obtained by changing the Cs-to-Mn molar feed ratio to 3:1.25 in the precursor solution. The XRD patterns of the as-prepared NCs are consistent with that of standard Cs_3MnBr_5 (PDF card No. 71-1416, Figure 1 f). The structure retrieve analysis reveals that Cs_3MnBr_5 NCs belong to space group of $I4/mcm$ (Figure 3 a) and have unit cell of $a = 9.598 \text{ \AA}$, $b = 9.598 \text{ \AA}$, $c = 15.567 \text{ \AA}$, $\alpha = 90^\circ$, $\beta = 90^\circ$, $\gamma = 90^\circ$ (Table S3). In this structure, each Mn^{2+} site is bonded to four bromine atoms, forming a $[\text{MnBr}_4]$ regular tetrahedron geometry. $[\text{MnBr}_4]$ unites are distributed along the c -axis direction and are separated by Cs^+ . TEM image shows that the as-prepared Cs_3MnBr_5 NCs have an average size of $15.5 \pm 1.7 \text{ nm}$ and a lattice distance of 0.178 nm , corresponding to the (251) crystal plane (Figures 1 g–i). It is noted that the as-prepared Cs_3MnBr_5 NCs may mix with a small amount of CsMnBr_3 , which is hard to distinguish by only using powder XRD (Discussed as below).

Next, optical properties of as-prepared CsMnBr_3 NCs and Cs_3MnBr_5 NCs are investigated. As shown in Figure 2 a, CsMnBr_3 NCs show a strong absorption peak at around

260 nm , which can be assigned to the low spin-forbidden transition from ${}^6\text{A}_1$ to ${}^4\text{A}_2$ of Mn^{2+} . Upon photoexcitation at 260 nm , CsMnBr_3 NCs show a red emission with peak position at 660 nm with FWHM of 91 nm and PLQY of 11% . The PL excitation (PLE) spectrum matches with the absorption spectrum. These peaks typically arise from the d-d transitions of octahedrally coordinated Mn^{2+} ions.^[24] CsMnBr_3 NCs show the same PL spectra with different excitation wavelengths and identical TRPL decays at different emission wavelengths. This suggests the different excited states generated with different excitation wavelengths funnel to the same emission state ${}^4\text{T}_1$ (Figures S2 and S3), then a transition from ${}^4\text{T}_1$ to the ground state ${}^6\text{A}_1$ leads to the red emission. Temperature-dependent PL spectra ($80\text{--}300 \text{ K}$) was further performed to study the optical properties (Figures S4 and S5). With decreasing temperature, the emission intensity gradually increases, which is resulted from a decrease in phonon-related nonradiative decay.^[25,26] A blue shift of the PL maximum is also observed with increasing temperature, which ascribes to the decrease in crystal-field strength and smaller splitting energy of the excited state caused by thermal expansion.^[26,27] As shown in Figure 2 b, the TR-PL spectrum of CsMnBr_3 NCs can be well fitted by a double-exponential function at room-temperature, yielding two lifetimes ($\tau_1 = 8.28 \text{ \mu s}$ and $\tau_2 = 206.48 \text{ \mu s}$) with average lifetime of 133.6 \mu s , while the PL decay prolongs at low temperature (Figure S5),

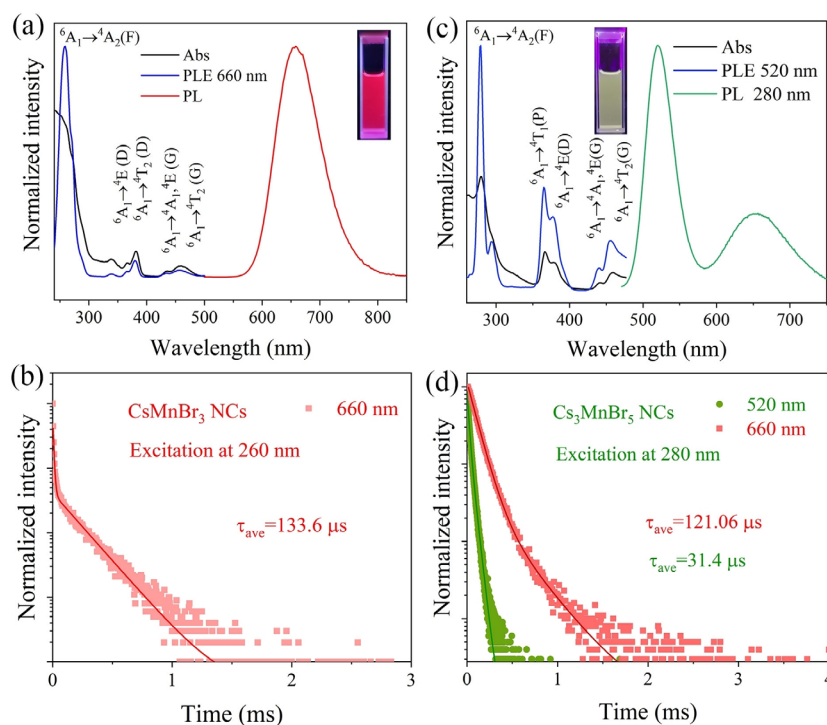


Figure 2. UV-Vis absorption, PLE, and PL spectra of (a) CsMnBr₃ NCs and (c) as-prepared Cs₃MnBr₅ NCs, respectively. The insets show the colloidal NCs under 254 nm and 365 nm UV light excitation, respectively. TR-PL decay curves of (b) CsMnBr₃ NCs and (d) as-prepared Cs₃MnBr₅ NCs at different emission wavelengths (520 nm and 660 nm) at 300 K.

which can be ascribed to the decreased non-radiative recombination at low temperature. The long lifetime with microsecond time scale is similar to CsMnBr₃ single crystals.^[28,29] We also noted that Bakr's et al. recently reported CsMnBr₃ NCs with picosecond lifetime.^[30] This may be due to PL lifetime of the Mn²⁺ d-d transitions is sensitive to the Mn-Mn distance, and the PL lifetime can be tuned from a few nanoseconds to milliseconds depending upon the Mn-Mn distance.^[30–32] In our work, the Mn-Mn distance in the CsMnBr₃ NCs along the c-axis is 3.24 Å, which is longer compared with Bakr's report (2.7 Å).^[30] The elongated Mn-Mn distance could lead to a coupled vibronic state like self-trapped exciton, which is the cause of long microsecond scale lifetime.^[33] The optical properties of CsMnBr₃ NCs with different Mn-Mn distances need further in-depth study, which is beyond the scope of this paper.

The optical properties of the as-synthesized Cs₃MnBr₅ NCs are also studied. The as-prepared NCs exhibit dual emission band at 520 nm and 660 nm upon excitation at 280 nm (Figure 2c). For the green emission band at 520 nm, which can be ascribed to the metal-centred d-d transition of the Mn²⁺ ion with a tetrahedral coordination geometry.^[34–36] As in different crystal field strengths, the luminescence of Mn²⁺ varies in a large range. In the weak field of tetrahedron coordination geometry, the luminescence of Mn²⁺ is usually green, while in the strong field of octahedron coordination geometry, the luminescence of Mn²⁺ is red.^[31,37] Three structured bands at 280, 365, and 460 nm are observed in the PLE spectrum at emission of 520 nm. The three bands originate from the energy splitting of the ⁴T₁ excited state in

Cs₃MnBr₅ structure. TR-PL results show that the 520 nm emission band has an average lifetime of 31.4 μs (Figure 2d). The relative short lifetime indicates that the non-radiative recombination is dominant in the as-prepared NCs, which results in low PLOQ of 6%.

For the 660 nm emission band, both the PL and PLE (Figure S7) spectra are similar to that of CsMnBr₃ NCs (Figure 2a), indicating that small amounts of CsMnBr₃ NCs may exist in the Cs₃MnBr₅ NCs, while it is hard to distinguish from XRD patterns. In addition, emission band at 660 nm shows two lifetimes (94.11 μs and 298.46 μs) with an average lifetime of 121.06 μs (Figure 2d). The TRPL decay curves of CsMnBr₃ NCs recorded at 660 nm show an excitation wavelength dependence (Figure S8). Excited states pumped by light with short wavelengths (high energy) show faster PL decay due to increased decay channels in high energy states compared to that in excited states pumped by light with longer wavelengths. Upon the same excitation wavelength, the as-prepared Cs₃MnBr₅ NCs at 660 nm emission band show similar PL lifetimes to that of the CsMnBr₃ NCs (Figure 2d and

Figure S8). These results confirm the co-existence of the CsMnBr₃ and Cs₃MnBr₅ phases in the as-prepared Cs₃MnBr₅ NCs. Hereinafter, we will combine the spectroscopy evidence with the XRD results to determine the phase transition of cesium manganese bromides NCs.

The pure-phase Cs₃MnBr₅ NCs can be obtained by immersing the as-prepared Cs₃MnBr₅ NCs in isopropanol for 5.5 h (details in SI). As one can see isopropanol treated Cs₃MnBr₅ NCs show a single emission band (at 520 nm) with a small FWHM of 43 nm, while the 660 nm emission band is disappeared (Figure 3b and Figure S9a). It is noted that the green emission (PLOQ of 48%) is improved compared to the as-prepared Cs₃MnBr₅ NCs, suggesting the non-radiative transition has been suppressed after the isopropanol treatment. In addition, TEM images display that the size of Cs₃MnBr₅ NCs gradually increased to ≈51 nm after the isopropanol treatment (Figure S10), which is larger compared to the as-prepared Cs₃MnBr₅ NCs (Figures 3d,e). This may be related to the re-growth of NCs during the phase transition from CsMnBr₃ to Cs₃MnBr₅. We also noted that the isopropanol treated Cs₃MnBr₅ NCs exhibit sharper XRD pattern than as-prepared Cs₃MnBr₅ NCs (Figures 1f and 3a). This indicates the Cs₃MnBr₅ NCs from isopropanol treatment have higher crystalline quality than the as-prepared Cs₃MnBr₅ NCs. After isopropanol treatment, TRPL results indicate that the green emission shows a prolonged PL lifetime (Figure 3c and Figure S9b), which ascribe to the decreased nonradiative recombination ratio due to improved crystal quality. So the improved PL properties of isopropanol treated NCs may be

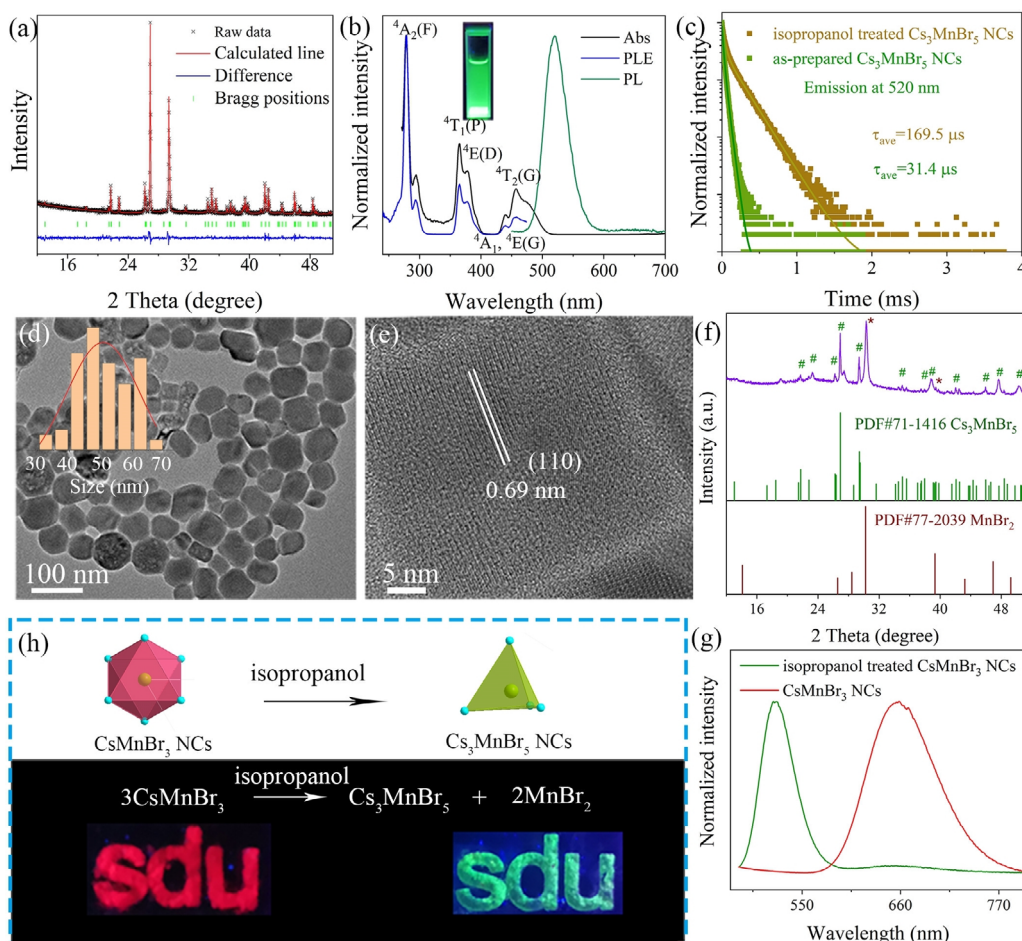


Figure 3. Rietveld refinement XRD patterns of (a) Cs_3MnBr_5 NCs. The observed data, calculation data, Bragg position and their difference are depicted with black cross, red solid line, green line and blue solid line. UV-Vis absorption, PLE, and PL spectra of (b) Cs_3MnBr_5 NCs. The insets show a photograph of the colloidal NCs under 365 nm UV light excitation. TR-PL decay curves of (c) isopropanol treated Cs_3MnBr_5 NCs and as-prepared Cs_3MnBr_5 NCs at 300 K. TEM image of (d) isopropanol treated Cs_3MnBr_5 NCs. The insets show size distribution histogram of Cs_3MnBr_5 NCs. (e) HRTEM image of a single Cs_3MnBr_5 NCs. XRD pattern of (f) isopropanol treated CsMnBr_3 NCs. Wells and asterisks denote signals from Cs_3MnBr_5 NCs and MnBr_2 in Figure 3 f, respectively. PL spectra of (g) isopropanol treated CsMnBr_3 NCs. (h) Schematic illustrations of the phase transformation process from CsMnBr_3 NCs to Cs_3MnBr_5 NCs. Photographs of (left) CsMnBr_3 NCs and (right) isopropanol treated CsMnBr_3 NCs are shown under 254 nm and 365 nm UV light, respectively.

related to decreased nonradiative transitions due to the improved crystalline quality.

To further study the phase transition process (from CsMnBr_3 to Cs_3MnBr_5 NCs) in isopropanol, we recorded the XRD and PL spectra at different reaction time during the phase transformation process. The XRD peak intensity of CsMnBr_3 NCs decreases with the increase of the peak intensity of Cs_3MnBr_5 and MnBr_2 (Figure 3 f and Figure S11). PL spectra show that the green emission band is enhanced while the red emission band is decreased (Figure 3 g and Figure S12). These results reveal that Cs_3MnBr_5 is a more stable phase than CsMnBr_3 in isopropanol and the CsMnBr_3 phase transforms to Cs_3MnBr_5 phase by stripping MnBr_2 (Figure 3 h).

Furthermore, we found that phase transition from CsMnBr_3 to $\text{Cs}_2\text{MnBr}_4 \cdot 2\text{H}_2\text{O}$ NCs could be triggered in a humid environment (Figure 4 a). When CsMnBr_3 NCs powders are placed in an environment with air humidity of 99% for several hours, a clear change in XRD patterns is

observed (Figures 4 b,d). The diffraction peaks can be indexed as triclinic $\text{Cs}_2\text{MnBr}_4 \cdot 2\text{H}_2\text{O}$ phase (PDF#50-0630) and some residue of MnBr_2 (Figure 4 d). The crystal structure of $\text{Cs}_2\text{MnBr}_4 \cdot 2\text{H}_2\text{O}$ was obtained by Rietveld refinement (Table S4 and Figure S13). The result demonstrates that each Mn atom is coordinated with four Br atoms and two water molecules to form an octahedron $[\text{MnBr}_4(\text{H}_2\text{O})_2]^{2-}$, and the octahedrons are isolated by Cs^+ (Figure S14). TEM study shows that the 0D $\text{Cs}_2\text{MnBr}_4 \cdot 2\text{H}_2\text{O}$ NCs have an average size of $\approx 16.6 \pm 3.2$ nm (Figure S15a). The $\text{Cs}_2\text{MnBr}_4 \cdot 2\text{H}_2\text{O}$ NCs show broad absorption with a tail extended to 720 nm (Figure S16, red line), which is different from that of spin-forbidden transition of Mn^{2+} in CsMnBr_3 NCs. This phenomenon is due to the existence of sub-band gap states.^[38] PL spectra depicts that $\text{Cs}_2\text{MnBr}_4 \cdot 2\text{H}_2\text{O}$ NCs have a blue emission peak at 440 nm with FWHM 81 nm and PLQY of 0.47% (Figure 4 e). The PL decay curves of $\text{Cs}_2\text{MnBr}_4 \cdot 2\text{H}_2\text{O}$ NCs (Figure S18, red line) are fitted by a double-exponential function ($\tau_1 = 0.48$ ns, $\tau_2 = 2.55$ ns), which is far shorter than

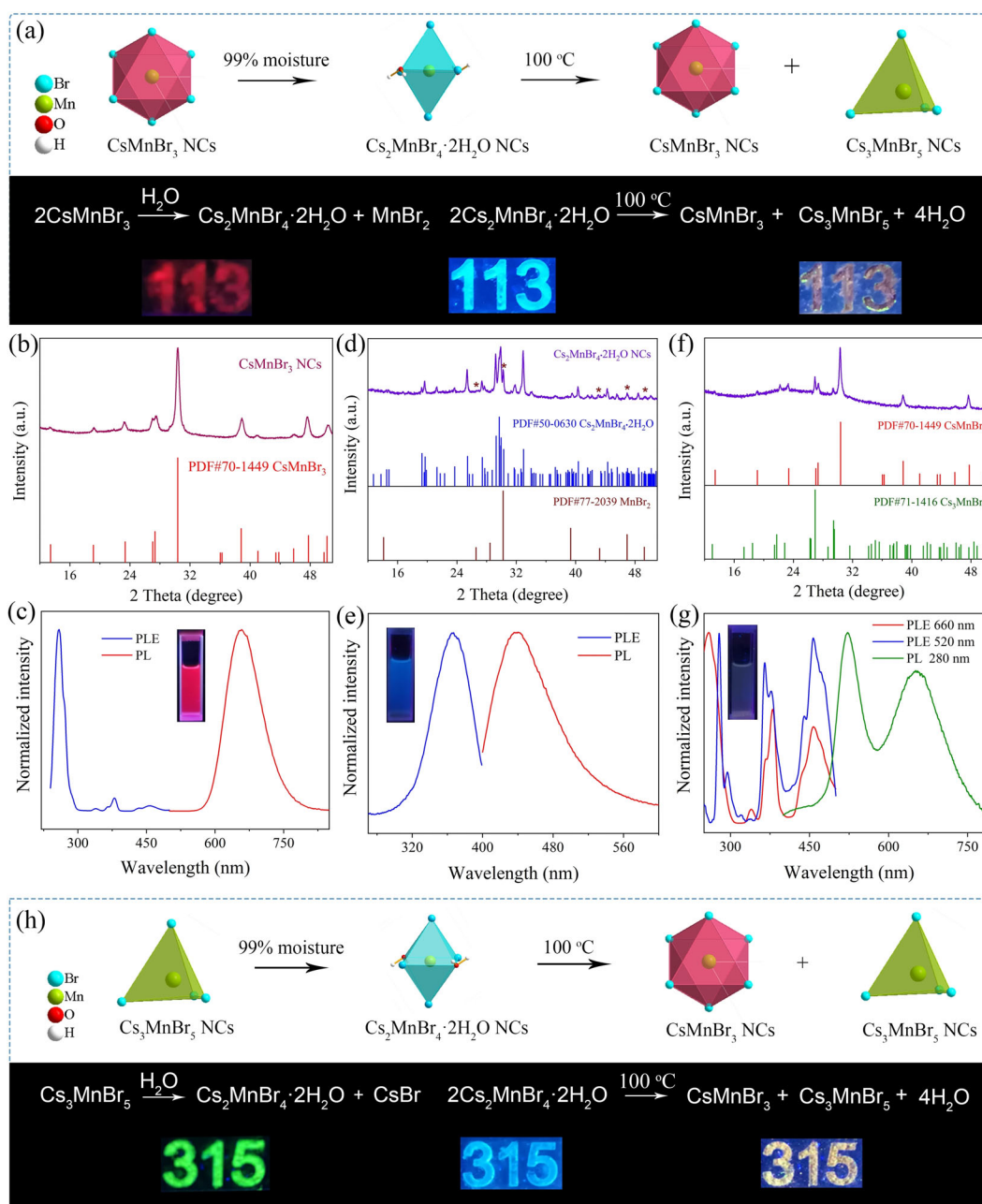


Figure 4. (a) Illustrations of the phase transformation process of CsMnBr_3 NCs and photographs of CsMnBr_3 NCs, $\text{Cs}_2\text{MnBr}_4 \cdot 2\text{H}_2\text{O}$ NCs and $\text{Cs}_2\text{MnBr}_4 \cdot 2\text{H}_2\text{O}$ NCs after heating at 100°C from left to right under 254 nm, 365 nm, 365 nm UV light. XRD patterns of (b) CsMnBr_3 NCs, (d) $\text{Cs}_2\text{MnBr}_4 \cdot 2\text{H}_2\text{O}$ NCs and (f) $\text{Cs}_2\text{MnBr}_4 \cdot 2\text{H}_2\text{O}$ NCs after heating at 100°C . Asterisks denote signals from MnBr_2 in Figure 4d. (left) PLE and (right) PL spectra of (c) CsMnBr_3 NCs, (e) $\text{Cs}_2\text{MnBr}_4 \cdot 2\text{H}_2\text{O}$ NCs and (g) $\text{Cs}_2\text{MnBr}_4 \cdot 2\text{H}_2\text{O}$ NCs after heating at 100°C . The insets show the colloidal NCs under 254 nm, 365 nm and 365 nm UV light excitation, respectively. (h) Schematic illustrations of the phase transformation process of Cs_3MnBr_5 NCs and photographs of Cs_3MnBr_5 NCs, $\text{Cs}_2\text{MnBr}_4 \cdot 2\text{H}_2\text{O}$ NCs and $\text{Cs}_2\text{MnBr}_4 \cdot 2\text{H}_2\text{O}$ NCs after heating at 100°C from left to right under 365 nm, 365 nm and 365 nm UV light on the glass slides.

the lifetime of CsMnBr_3 NCs. It is possibly originated from the existence of sub-band gap states and a strong electron-phonon coupling as the presence of the O-H stretching vibration mode in H_2O molecules. The strong electron-phonon coupling can lead to multi-phonon decay, the reduced lifetime and low PLQY.^[39,40] Similarly, water can also trigger the phase transformation of Cs_3MnBr_5 NCs to $\text{Cs}_2\text{MnBr}_4 \cdot 2\text{H}_2\text{O}$ (PDF#50-0630) (Figure S19). In contrast with $\text{Cs}_2\text{MnBr}_4 \cdot 2\text{H}_2\text{O}$ NCs transformed from CsMnBr_3 NCs,

the absorption spectra of Cs_3MnBr_5 NCs transformed $\text{Cs}_2\text{MnBr}_4 \cdot 2\text{H}_2\text{O}$ NCs have the relatively shorter absorption tail (Figure S16, green line) and higher PLQY of 1.29%, which possibly ascribe to the reduced sub-band gap states due to larger size. $\text{Cs}_2\text{MnBr}_4 \cdot 2\text{H}_2\text{O}$ NCs could inversely transform into the mixture of CsMnBr_3 and Cs_3MnBr_5 phase during the thermal annealing dehydration step. When $\text{Cs}_2\text{MnBr}_4 \cdot 2\text{H}_2\text{O}$ NCs were heated at 100°C for 1 h in ambient atmosphere, phase structure of CsMnBr_3 NCs and Cs_3MnBr_5 NCs were

clearly observed in XRD patterns (Figure 4f and Figure S19e). XRD patterns show that $\text{Cs}_2\text{MnBr}_4 \cdot 2\text{H}_2\text{O}$ NCs after heating at 100°C generate different amounts of CsMnBr_3 NCs and Cs_3MnBr_5 NCs, which result in different emission color under UV light excitation. In addition, the PL spectrum has dual emission band at 520 nm and 660 nm upon excitation at 280 nm, which is consistent with the characteristic emission peaks of CsMnBr_3 NCs and Cs_3MnBr_5 NCs, respectively (Figure 4g). PLE and TRPL spectra of 660 nm and 520 nm emission band are consistent with that of CsMnBr_3 NCs and Cs_3MnBr_5 NCs (Figures S20–S22), respectively. These results suggest a successful transformation from blue-luminescent $\text{Cs}_2\text{MnBr}_4 \cdot 2\text{H}_2\text{O}$ NCs to a mixed phase of CsMnBr_3 NCs and Cs_3MnBr_5 NCs. The mixture of CsMnBr_3 and Cs_3MnBr_5 phase can be transformed to Cs_3MnBr_5 structure with isopropanol treatment, indicating that the phase transition process is reversible (Figure S23). Furthermore, we have also listed the basic optical properties of common lead-free perovskite NCs for comparison (Table S5). Different from previous reported lead-free perovskite NCs which exhibit broadband PL, the cesium manganese bromides NCs exhibit relative narrower PL band with high color purity, which show great potential for display applications.

In summary, we successfully developed a phase transition strategy to engineer cesium manganese bromides NCs with a wide range color-tunable emission and high color purity. This proposed strategy is important in adjusting photoluminescence wavelength and obtaining the stability of NCs against destruction by air and water. Additionally, the tunable PL color provides a novel and unique approach for the application of this material in anti-counterfeiting.

Acknowledgements

This work was supported by the National Key Research and Development Program of China (grant 2017YFA0204800), the National Natural Science Foundation of China (Grant Nos. 21833009, 22088102, 21525315, 22005295), DICP I202017, the Scientific Instrument Developing Project of the Chinese Academy of Sciences (Grant No. YJKYYQ20190003), Liao Ning Revitalization Talents Program (XLYC1802126), the Dalian City Foundation for Science and Technology Innovation (2019J12GX031). This work is supported by the Project funded by China Postdoctoral Science Foundation (2020M682159). B. Yang acknowledges the funding support from the Youth Innovation Promotion Association CAS (2021183). We would like to thank Xiaojun Li and Haiyan Sui from Shandong University Core Facilities for Life and Environmental Sciences for their help with the TEM.

Conflict of Interest

The authors declare no conflict of interest.

Keywords: cesium manganese bromides · color-tunable emission · lead-free perovskite · nanocrystals

- [1] X. Zhang, X. Wu, X. Liu, G. Chen, Y. Wang, J. Bao, X. Xu, X. Liu, Q. Zhang, K. Yu, W. Wei, J. Liu, J. Xu, H. Jiang, P. Wang, X. Wang, *J. Am. Chem. Soc.* **2020**, *142*, 4464–4471.
- [2] H. Guan, S. Zhao, H. Wang, D. Yan, M. Wang, Z. Zang, *Nano Energy* **2020**, *67*, 104279.
- [3] F. Xu, K. Meng, B. Cheng, S. Wang, J. Xu, J. Yu, *Nat. Commun.* **2020**, *11*, 4613.
- [4] J. Chen, K. Židek, P. Chábera, D. Liu, P. Cheng, L. Nuuttila, M. J. Al-Marri, H. Lehtivuori, M. E. Messing, K. Han, K. Zheng, T. J. Pullerits, *J. Phys. Chem. Lett.* **2017**, *8*, 2316–2321.
- [5] J. Chen, P. Chábera, T. Pascher, M. E. Messing, R. Schaller, S. Canton, K. Zheng, T. Pullerits, *J. Phys. Chem. Lett.* **2017**, *8*, 5119–5124.
- [6] S. Toso, D. Baranov, L. Manna, *Acc. Chem. Res.* **2021**, *54*, 498–508.
- [7] L. Protesescu, S. Yakunin, M. I. Bodnarchuk, F. Krieg, R. Caputo, C. H. Hendon, R. X. Yang, A. Walsh, M. V. Kovalenko, *Nano Lett.* **2015**, *15*, 3692–3696.
- [8] J. Zhang, G. Hodes, Z. Jin, S. Liu, *Angew. Chem. Int. Ed.* **2019**, *58*, 15596–15618; *Angew. Chem.* **2019**, *131*, 15742–15765.
- [9] V. K. Ravi, G. B. Markad, A. Nag, *ACS Energy Lett.* **2016**, *1*, 665–671.
- [10] K. Lin, J. Xing, L. N. Quan, F. P. G. de Arquer, X. Gong, J. Lu, L. Xie, W. Zhao, D. Zhang, C. Yan, W. Li, X. Liu, Y. Lu, J. Kirman, E. H. Sargent, Q. Xiong, Z. Wei, *Nature* **2018**, *562*, 245–248.
- [11] Z. Li, Z. Chen, Y. Yang, Q. Xue, H.-L. Yip, Y. Cao, *Nat. Commun.* **2019**, *10*, 1027.
- [12] J. Chen, D. Liu, M. J. Al-Marri, L. Nuuttila, H. Lehtivuori, K. Zheng, *Sci. China Mater.* **2016**, *59*, 719–727.
- [13] H. Arfin, J. Kaur, T. Sheikh, S. Chakraborty, A. Nag, *Angew. Chem. Int. Ed.* **2020**, *59*, 11307–11311; *Angew. Chem.* **2020**, *132*, 11403–11407.
- [14] B. Yang, X. Mao, F. Hong, W. Meng, Y. Tang, X. Xia, S. Yang, W. Deng, K. Han, *J. Am. Chem. Soc.* **2018**, *140*, 17001–17006.
- [15] B. Yang, K. Han, *Acc. Chem. Res.* **2019**, *52*, 3188–3198.
- [16] Q. Fan, G. V. Biesold-McGee, J. Ma, Q. Xu, S. Pan, J. Peng, Z. Lin, *Angew. Chem. Int. Ed.* **2020**, *59*, 1030–1046; *Angew. Chem.* **2020**, *132*, 1042–1059.
- [17] S. Liu, B. Yang, J. Chen, D. Wei, D. Zheng, Q. Kong, W. Deng, K. Han, *Angew. Chem. Int. Ed.* **2020**, *59*, 21925–21929; *Angew. Chem.* **2020**, *132*, 22109–22113.
- [18] C. Kang, H. Rao, Y. Fang, J. Zeng, Z. Pan, X. Zhong, *Angew. Chem. Int. Ed.* **2021**, *60*, 660–665; *Angew. Chem.* **2021**, *133*, 670–675.
- [19] X. Li, X. Gao, X. Zhang, X. Shen, M. Lu, J. Wu, Z. Shi, V. L. Colvin, J. Hu, X. Bai, W. W. Yu, Y. Zhang, *Adv. Sci.* **2021**, *8*, 2003334.
- [20] P. Cheng, L. Sun, L. Feng, S. Yang, Y. Yang, D. Zheng, Y. Zhao, Y. Sang, R. Zhang, D. Wei, W. Deng, K. Han, *Angew. Chem. Int. Ed.* **2019**, *58*, 16087–16091; *Angew. Chem.* **2019**, *131*, 16233–16237.
- [21] M. Leng, Y. Yang, Z. Chen, W. Gao, J. Zhang, G. Niu, D. Li, H. Song, J. Zhang, S. Jin, J. Tang, *Nano Lett.* **2018**, *18*, 6076–6083.
- [22] J. Sun, J. Yang, J. I. Lee, J. H. Cho, M. S. Kang, *J. Phys. Chem. Lett.* **2018**, *9*, 1573–1583.
- [23] S. Li, J. Xu, Z. Li, Z. Zeng, W. Li, M. Cui, C. Qin, Y. Du, *Chem. Mater.* **2020**, *32*, 6525–6531.
- [24] Y. Rodríguez-Lazcano, L. Nataf, F. Rodríguez, *Phys. Rev. B* **2009**, *80*, 085115.
- [25] X. Yuan, S. Ji, M. C. De Siena, L. Fei, Z. Zhao, Y. Wang, H. Li, J. Zhao, D. R. Gamelin, *Chem. Mater.* **2017**, *29*, 8003–8011.
- [26] W. Wu, W. Liu, Q. Wang, Q. Han, Q. Yang, *J. Alloys Compd.* **2019**, *787*, 165–172.

- [27] K. Xu, C. C. Lin, X. Xie, A. Meijerink, *Chem. Mater.* **2017**, *29*, 4265–4272.
- [28] R. L. Blakley, C. E. Martinez, M. F. Herman, G. L. McPherson, *Chem. Phys.* **1990**, *146*, 373–380.
- [29] G. L. McPherson, Y. Y. Waguespack, T. C. Vanoy, W. J. Rodriguez, *J. Chem. Phys.* **1990**, *92*, 1768–1774.
- [30] J. Almutlaq, W. J. Mir, L. Gutiérrez-Arzaluz, J. Yin, S. Vasylevskyi, P. Maity, J. Liu, R. Naphade, O. F. Mohammed, O. M. Bakr, *ACS Mater. Lett.* **2021**, *3*, 290–297.
- [31] V. Morad, I. Cherniukh, L. Pöttschacher, Y. Shynkarenko, S. Yakunin, M. V. Kovalenko, *Chem. Mater.* **2019**, *31*, 10161–10169.
- [32] C. Li, X. Bai, Y. Guo, B. Zou, *ACS Omega* **2019**, *4*, 8039–8045.
- [33] X. Bai, H. Zhong, B. Chen, C. Chen, J. Han, R. Zeng, B. J. Zou, *J. Phys. Chem. C* **2018**, *122*, 3130–3137.
- [34] B. Su, M. S. Molokeev, Z. Xia, *J. Mater. Chem. C* **2019**, *7*, 11220–11226.
- [35] L.-J. Xu, S. Lee, X. Lin, L. Ledbetter, M. Worku, H. Lin, C. Zhou, H. Liu, A. Plaviak, B. Ma, *Angew. Chem. Int. Ed.* **2020**, *59*, 14120–14123; *Angew. Chem.* **2020**, *132*, 14224–14227.
- [36] M. Li, Z. Xia, *Chem. Soc. Rev.* **2021**, *50*, 2626–2662.
- [37] L. Tan, Z. Luo, X. Chang, Y. Wei, M. Tang, W. Chen, Q. Li, P. Shen, Z. Quan, *Inorg. Chem.* **2021**, *60*, 6600–6606.
- [38] B. Yang, J. Chen, F. Hong, X. Mao, K. Zheng, S. Yang, Y. Li, T. Pullerits, W. Deng, K. Han, *Angew. Chem. Int. Ed.* **2017**, *56*, 12471–12475; *Angew. Chem.* **2017**, *129*, 12645–12649.
- [39] W. Jia, R. Brundage, W. J. P. R. B. Yen, *Phys. Rev. B* **1983**, *27*, 41–45.
- [40] H. Xiao, P. Dang, X. Yun, G. Li, Y. Wei, Y. Wei, X. Xiao, Y. Zhao, M. S. Molokeev, Z. Cheng, J. Lin, *Angew. Chem. Int. Ed.* **2021**, *60*, 3699–3707; *Angew. Chem.* **2021**, *133*, 3743–3751.

Manuscript received: April 20, 2021

Revised manuscript received: May 27, 2021

Accepted manuscript online: June 20, 2021

Version of record online: ■■■■■■, ■■■■■■

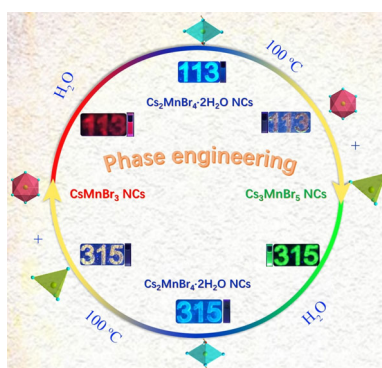
Communications



Nanocrystals

Q. Kong, B. Yang,* J. Chen, R. Zhang,
S. Liu, D. Zheng, H. Zhang, Q. Liu,
Y. Wang, K. Han* ———— ■■■■-■■■■

Phase Engineering of Cesium Manganese
Bromides Nanocrystals with Color-
Tunable Emission



We developed a unique phase transition strategy to engineer the emission color of lead-free cesium manganese bromides nanocrystals, which achieve a tunable red/green/blue emission with high color purity.